

ROOM-TEMPERATURE PPB-LEVEL ANILINE VAPOR SENSOR FUNCTIONALIZED WITH UIO-66-SO₃HJun Cai^a, Luyu Wang^{a,*} and Yunling Wu^b^aCollege of Artificial Intelligence and E-Commerce, Zhejiang Gongshang University Hangzhou College of Commerce, Hangzhou 311599, China^bInstitute of Functional Nano and Soft Materials, Jiangsu Key Laboratory for Carbon-Based Functional Materials and Devices, Soochow University, Suzhou 215123, China

Recebido em 11/06/2022; aceito em 22/09/2022; publicado na web em 20/10/2022

Aniline vapor must be immediately detected at low concentrations since it is a hazardous gaseous chemical. Here, ppb level aniline vapor is detected using the metal-organic framework of UIO-66-SO₃H. Utilizing a quartz crystal microbalance (QCM) sensing platform, the aniline adsorption-induced mass change of UIO-66-SO₃H is converted to a signal of frequency shift. The sensor can detect a concentration of 20 ppb of aniline vapor and has good sensitivity for this purpose. Additionally, the sensor's repeatability and stability are satisfactory. Notably, the sensor's selectivity is prominent. Its response to aniline is much higher than that of ten interfering gases and BTEX vapor. And even in conditions with varying levels of humidity, this sensor maintains response stability.

Keywords: gas sensor; sensitivity; QCM; aniline; MOFs.

INTRODUCTION

As a typical volatile organic compound (VOC), aniline is frequently utilized as a raw material for the production of resins, medications, and azo dyes.¹⁻³ Recently, azo dyes are usually applied in plastic, paint, and colored fabrics. However, azo dyes progressively produce the byproducts of their breakdown, such as the cancer-causing aniline.⁴ To make matters worse, Sudan red is even illegally used in the food industry to enhance the freshness of food, and toxic aniline is one of the raw materials of Sudan red.⁵ Therefore, real-time detection of highly toxic aniline vapors is necessary especially at the parts per billion (ppb) level.⁶⁻⁸ Currently, high-performance gas chromatography-mass spectrometers and fluorescence sensors, which are large, time-consuming, and immobile, are the major tools used for aniline detection.⁹⁻¹¹ Compared with the above unsatisfactory instruments, gas sensors have the merits of easy to use, small volume, low cost, and portable.¹²⁻¹⁴ Nonetheless, the sensitivity of the chemical sensor used to detect aniline vapor still can not meet the practical application, and usually can only detect the ppm (parts per million) concentration level.¹⁵⁻¹⁹ Therefore, a gas sensor must be created in order to detect aniline vapor at ppb concentration levels.

In order to solve the problem of poor sensitivity, sensing materials with ultra-high specific surface area and abundant sensing positions are essential.²⁰⁻²² From this point of view, the metal-organic frameworks (MOF) material with ultra-high specific surface area is an ideal candidate material.²³⁻²⁷ In fact, MOF materials have shown considerable capabilities in molecular capture/storage and have been widely used as gas adsorbents.²⁸⁻³⁰ The insulating properties of MOF materials make them difficult to construct traditional chemical resistance gas sensors.³¹ Fortunately, mass-sensitive chemical sensors such as quartz crystal microbalance (QCM) or resonant cantilever can be used to convert adsorbing gas induced mass-change to detect signals.³²⁻³⁴ In this study, QCM is used as an example to illustrate the working mechanism of a mass-type chemical sensor. Due to the gas molecules' adsorption, the mass of the sensing material increased appropriately. The mass increase (Δm) causes the frequency shift (Δf) of the QCM. If the mass increase is much smaller than the inherent

mass of the QCM, the QCM can output a frequency shift signal Δf proportionally to the additional mass of the sensing material.³⁵⁻³⁷ Based on the above-mentioned working mechanism, nanoporous materials such as MOF are beneficial to be used as mass-sensitive materials due to their ultra-high specific surface area, abundant specific adsorption sites and large molecular capture/storage volume.³⁸⁻⁴⁰ Based on the resonant cantilever or QCM, some reports have proved the sensing application of MOF materials, such as MIL-101, Ni-MOF-74, and MOF-199.⁴¹⁻⁴³

UIO-66-SO₃H is a derivative of UIO-66. UIO-66-SO₃H is used in proton transfer, water treatment, and other applications, but its performance in gas sensing based on QCM platform has not been explored.⁴⁴⁻⁴⁶ In this work, UIO-66-SO₃H crystals are employed as mass-sensitive material for ppb-level aniline vapor detection based on QCM platform. The prepared UIO-66-SO₃H crystals are characterized via using instrumental analytical methods, and the characterization results indicate that the prepared UIO-66-SO₃H crystals have an ultrahigh surface area. The fabricated sensor exhibits satisfactory sensing performance to the target aniline molecules because of the extremely high specific surface area and -SO₃H group.

EXPERIMENTAL

Materials

2-sulfo terephthalic acid was obtained from Alfa Aesar. All the other reagents were purchased from Sinopharm Chemical Reagent Co. Ltd. Silver electrode QCM resonators were purchased from Chengdu Westsensor Co., China. The commercial UIO-66 was purchased from Zhengzhou Feynman-nano-technology Co. Ltd.

Synthesis of UIO-66-SO₃H

0.615 mmol (151.4 mg) 2-sulfo terephthalic acid (98% purity) as the organic ligand was solved in 25 mL DMF (AR, 99.5%). Meanwhile, 0.615 mmol (143.3 mg) of zirconium chloride ($\geq 99.9\%$) was solved in 25 mL of DMF. Then, the two solutions were mixed evenly, and 6 mL acetic acid ($\geq 99.9\%$) was added. After ultrasonic treatment, the mixed solution was solvothermally treated at 120 °C

*e-mail: dr.luyu-wang@hotmail.com

for 4 h. After several times of ethanol (AR, 99.7%) cleaning and centrifugation, the obtained material was soaked in methanol (AR, 99.5%) for three days, and the methanol solution was updated every day. Finally, the solid powder of UiO-66-SO₃H was obtained by placing the material in a vacuum oven at 60 °C for 12 hours.

Characterization

Powder X-ray diffraction data was obtained on a Panalytical X'Pert 3 Powder advance diffractometer with a graphite-monochromatized CuK α radiation. Brunauer-Emmett-Teller (BET) method was used to calculate the specific surface areas. The N₂ adsorption-desorption isotherms at 77 K were measured on a Micromeritics ASAP 2460 system to evaluate their pore structures. The surface morphology of the material was observed by the Zeiss Sigma300 scanning electron microscope (SEM). For the characterization of the functional groups, we employed Fourier-transform infrared spectroscope (FTIR, Thermo Scientific Nicolet iS20, Thermo Fisher Scientific). Elemental analyses for the material were implemented with Vario Micro Cube Elemental Analyzer.

Fabrication and test method of QCM Sensor

Supporting Information provides a detailed description of the sensor's fabrication and testing procedures, which are based on prior literature.⁴⁷ Figure 1S in Supporting Information shows the schematic of the testing system.

RESULTS AND DISCUSSION

Materials characterization

First, powder XRD is used to characterize the prepared UiO-66-SO₃H material in order to ensure that the -SO₃H functionalization did not influence the structural crystallinity of UiO-66. As shown in Figure 1a, the XRD peaks of UiO-66-SO₃H are well matched with the simulated UiO-66 and published results of UiO-66-SO₃H material, indicating that the synthesis of UiO-66-SO₃H was successful.^{44,48} It is indicating that the -SO₃H functionalization only slightly affects the crystallization degree of UiO-66, but has no effect on crystal structure. In addition, there is no other obvious peak appeared in the XRD pattern of UiO-66-SO₃H, which is indicative of its high level of purity. The sharp diffraction peaks in XRD pattern indicate that the prepared UiO-66-SO₃H material has high degree of crystallinity. The high crystallinity represents superior quality and stability of the prepared UiO-66-SO₃H material in this work.

The nature and structural properties of UiO-66-SO₃H were characterized in this work using FTIR spectral analysis, as shown in Figure 1b. The FTIR spectrum of the prepared UiO-66-SO₃H reveals that two apparent absorption bands at 1585.87 cm⁻¹ and 1412.68 cm⁻¹ were observed, which might affirm the existence of building block units formed by the coordination reaction between carboxyl groups of 2-sulfo terephthalic acid and zirconium nodes in the prepared UiO-66-SO₃H. The absorption band at 774.08 cm⁻¹ could be ascribed to the C-C ring out-of-plane bending nodes in the UiO-66-SO₃H. A small absorption band at 1235.72 cm⁻¹ was matched to the O=S=O symmetric stretching modes, while the absorption band at 1077.24 cm⁻¹ might be due to stretching vibrations of S-O.⁴⁹ The results showed that the introduction of -SO₃H into UiO-66-SO₃H was successful.

SEM imaging makes a significant contribution to understanding the surface morphology of the prepared UiO-66-SO₃H material. The surface, size, and shape of the crystals can be observed based on the collection from SEM. Figure 2a shows the SEM image of the prepared UiO-66-SO₃H material. A crystalline structure supported with particles exhibiting an octahedral shape with size within the range of (300 nm-400 nm) could be seen in this image. As shown in Figure 2b-f, elements Zr, C, O, and S were detected successfully in UiO-66-SO₃H by energy dispersive X-ray spectrometry (EDX) analysis, proving that the -SO₃H group was introduced into the UiO-66 framework. The values of elemental analysis are listed as follows: C (25.92%), H (1.35%), O (38.28%) and S (8.89%). According to the theoretical calculation of the structural formula of UiO-66-SO₃H (C₄₈H₂₂O₅₀S₆Zr₆H₆), the elemental percentage values are C (26.87%), H (1.31%), O (37.33%) and S (8.96%), respectively. Results of comparisons indicate that the two sets of values mentioned above are nearly identical.

The structure information of UiO-66-SO₃H, including BET surface area, pore volume, and pore size, was investigated based on experimental data of nitrogen (N₂) adsorption-desorption isotherms. The adsorption-desorption isotherm is depicted in Figure 3 as a combination of types I and IV, demonstrating the simultaneous existence of micropore and mesopore.⁵⁰ As shown in the table in Figure 3, the average pore size of UiO-66-SO₃H is 1.760 nm. The BET surface area of UiO-66-SO₃H is 763.4 m² g⁻¹. The total pore volume of UiO-66-SO₃H is 0.3366 mL g⁻¹. Therefore, the introduction of -SO₃H group did not change the original porous structure of UiO-66, and still appeared as a microporous feature.

Gaseous aniline sensing properties

Here, UiO-66-SO₃H material is modified onto the QCM chip using the drop coating method technology to create a mass-type sensor.

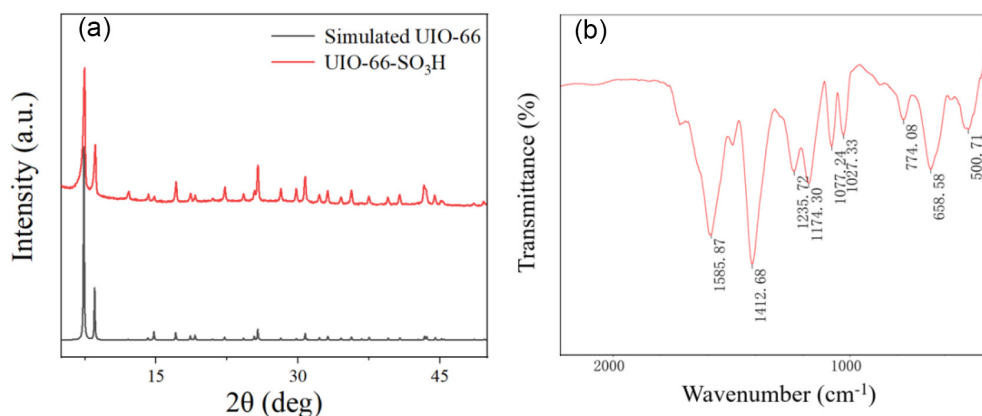


Figure 1. (a) XRD patterns of UiO-66-SO₃H and simulated UiO-66. (b) FTIR spectrum of UiO-66-SO₃H

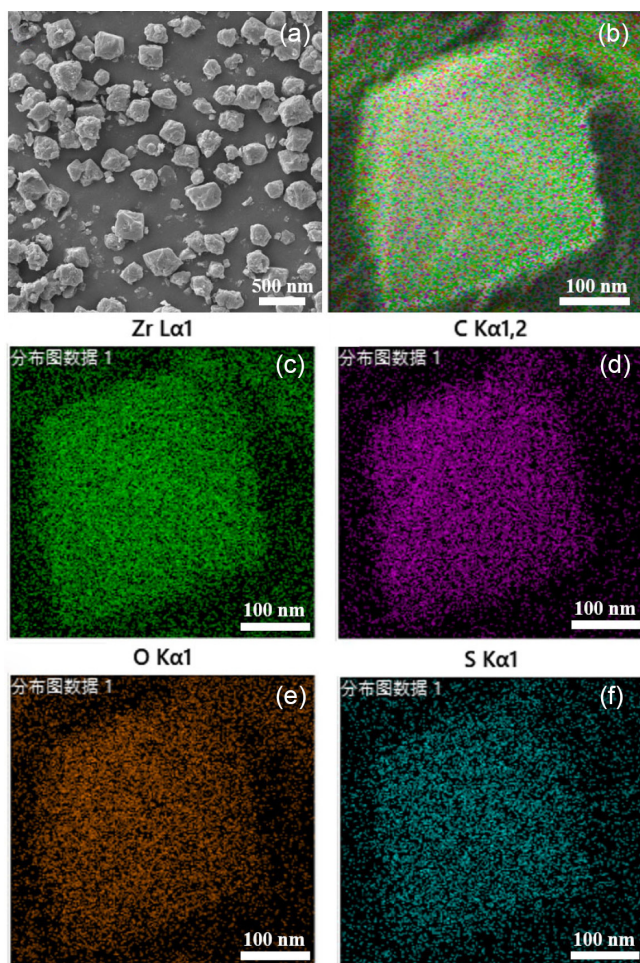


Figure 2. (a) SEM image of UiO-66-SO₃H. (b-f) Elemental mapping characterization of the prepared UiO-66-SO₃H, including Zr, C, O, and S

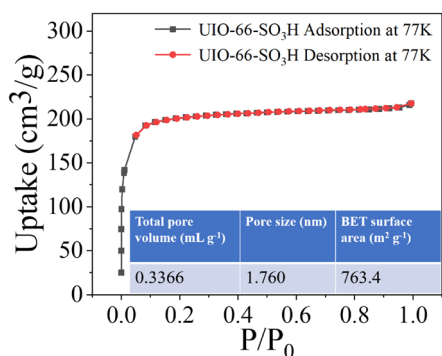


Figure 3. The nitrogen sorption isotherm of UiO-66-SO₃H at 77 K

The finished UiO-66-SO₃H based QCM sensor is then placed inside the sensing testing chamber at room temperature for the subsequent evaluation of the sensing performance. Aniline molecules adsorb to the UiO-66-SO₃H sensing material when the UiO-66-SO₃H based QCM sensor is exposed to an atmosphere containing aniline vapor, adding mass (Δm) to the sensing material. The frequency of the sensor proportionally decreases as a result of Δm leading the frequency shift (Δf). Figure 4a presents the frequency shift of two kinds of QCM sensors based on various sensing materials, including UiO-66-SO₃H and commercial UiO-66 towards 40, 60, 70 and 120 ppb aniline vapor at 298 K. It can be observed that the UiO-66-SO₃H based QCM sensor exhibits an obviously larger response under various concentrations of aniline vapor. This should be attributed to the -SO₃H group.

The real-time and continuous sensing curve in Figure 4b records the frequency shift of the UiO-66-SO₃H based QCM sensor along with the concentrations of aniline vapor in the range of 20 to 120 ppb. It is obvious that the UiO-66-SO₃H based QCM sensor is capable of detecting aniline vapor with a concentration of 20 ppb. As illustrated in Figure 4c, the real-time and continuous sensing curve can be further turned into an isotherm (the relationship of frequency shift versus the concentration of aniline vapor). It is clear that the frequency shift and the amount of aniline vapor present a Langmuir relationship.

To illustrate the response speed of the UiO-66-SO₃H based QCM sensor, the response time that represents the response time from fundamental frequency to 90% of the final frequency state is herein quantitatively obtained.⁵¹ According to the experimental sensing curve, which is depicted in Figure 4d, the value of the response time is as short as 74 s to 120 ppb of aniline vapor, demonstrating the quick response-speed of the UiO-66-SO₃H based QCM sensor. Moreover, the recovery time is defined as the time to achieve 90% of the recovery frequency shift. The recovery time is 296 s approximately.

For evaluating the selectivity of the UiO-66-SO₃H based QCM sensor, ten kinds of common gases including H₂, SO₂, CO₂, H₂S, O₂, CO, NH₃, 1-hexanamine, amylamine and butylamine are selected as interfering gases. The frequency shift data in Figure 5a indicate that the UiO-66-SO₃H based QCM sensor outputs smaller than 2.3 Hz frequency-shift to all the ten kinds of interfering gases with the concentration of 60 ppb. By contrast, the frequency shift of the UiO-66-SO₃H based QCM sensor to aniline vapor with the concentration of 60 ppb is as high as 7.9 Hz. Besides the target aniline vapor, the UiO-66-SO₃H based QCM sensor outputs the highest response to 1-hexanamine, amylamine and butylamine than the other seven kinds of interfering gases. It is known that 1-hexanamine, amylamine and butylamine are basic gases. Basic gas molecule tends to adsorb on the -SO₃H group in UiO-66-SO₃H. However, 1-hexylamine, amylamine, butylamine and aniline molecules are all basic gases, and there is no obvious difference in the molecular weight of the above four gases. Therefore, the acid-base adsorption between UiO-66-SO₃H and amino group in 1-hexylamine, amylamine, butylamine and aniline caused some frequency shift, but the unique benzene ring structure of aniline molecule and the benzene ring structure in UiO-66-SO₃H tend to π - π adsorption and contribute more significant frequency shift.

In order to investigate the effect of relative humidity (RH) on aniline sensing in terms of another selectivity indicator, the frequency shift data of the UiO-66-SO₃H based QCM sensor to 60 ppb aniline vapor were taken under different %RH including 30%, 40%, 60%, 70%, 80% and 90%. Figure 5b shows the frequency shift of the QCM sensor based on the UiO-66-SO₃H. The frequency shift of the UiO-66-SO₃H based QCM sensor to aniline vapor varied little with an increase in RH. These findings showed that the UiO-66-SO₃H based QCM sensor performed well at various humidity levels. It should be attributed to the hydrophobic benzene ring structure of the aniline molecule.

Investigations are also made on the repeatability of QCM sensors based on UiO-66-SO₃H. Figure 6a plots a typical successive sensing curve of the UiO-66-SO₃H based QCM sensor to 20 ppb of aniline vapor for three times. The frequency shift of the UiO-66-SO₃H-based QCM sensor to aniline vapor is measured as 2.04, 2.05, and 2.03 Hz, respectively, and exhibits good reproducibility.

By analyzing the frequency shift of the same sensor six times over the course of six weeks, the long-term stability of the UiO-66-SO₃H based QCM sensor was examined.

The long-term stability of the UiO-66-SO₃H based QCM sensor is investigated via testing the frequency shift of the same sensor for six times in a six-week period. The UiO-66-SO₃H based QCM sensor

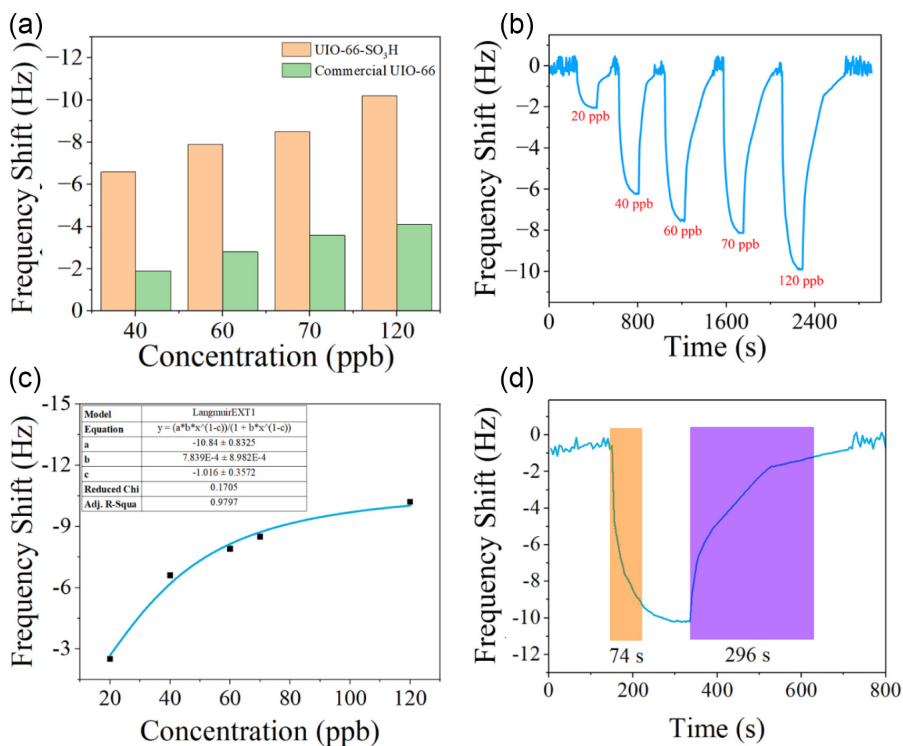


Figure 4. (a) Frequency shift of UIO-66-SO₃H and commercial UIO-66 based QCM sensors to aniline with various concentrations. (b) Detection curve of the UIO-66-SO₃H based QCM sensor to aniline vapor compared with various concentrations, including 20 ppb, 40 ppb, 60 ppb, 70 ppb, and 120 ppb. (c) The transformed relationship between the aniline concentration and frequency shift, which fits well with the function of the Langmuir equation for the UIO-66-SO₃H based QCM sensor. (d) The response time and recovery time of the UIO-66-SO₃H based QCM sensor to 120 ppb aniline vapor

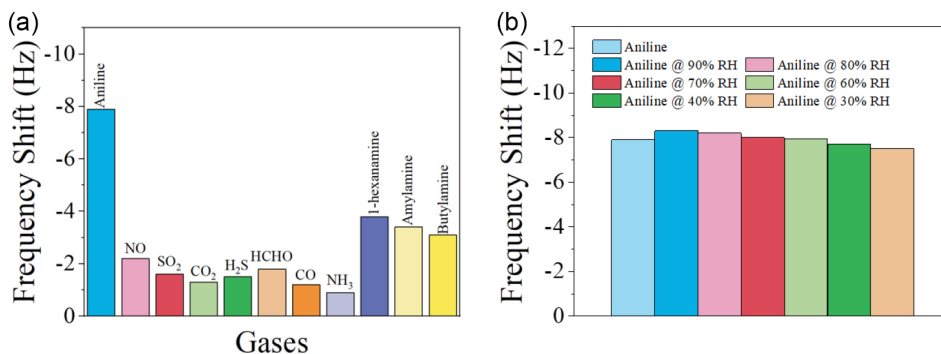


Figure 5. (a) Selectivity of the UIO-66-SO₃H based QCM sensor to eleven different gases. The concentrations of ten kinds of interfering gases are 60 ppb, and that of aniline vapor is 60 ppb, too. (b) Response shift of UIO-66-SO₃H based QCM sensor towards 60 ppb aniline under different relative humidity

outputs 7.90 Hz frequency shift to 60 ppb of aniline vapor during the initial testing, as illustrated in Figure 6b. The UIO-66-SO₃H based QCM sensor is regularly tested to aniline vapor with an equal

concentration of 60 ppb after six weeks. According to the research results, the final detection after six weeks had a response of 7.42 Hz, indicating a minimal decline in frequency shift.

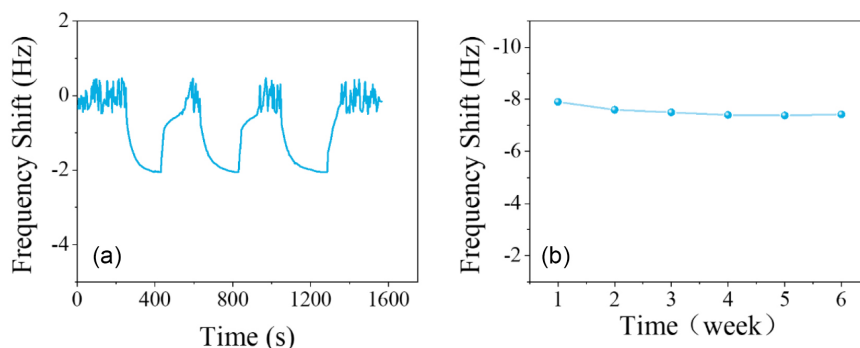


Figure 6. (a) Three cycles of frequency shift to aniline vapor with a constant concentration of 20 ppb. (b) Long-term (six weeks) stability evaluation of the UIO-66-SO₃H based QCM sensor for the detection of 60 ppb aniline vapor

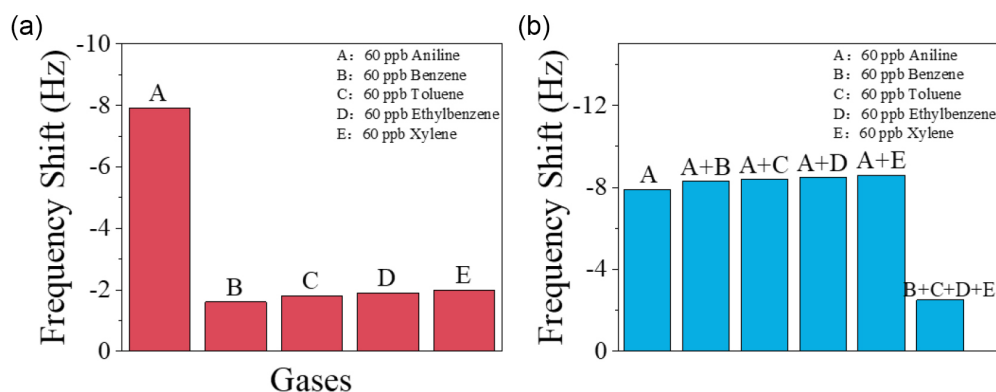


Figure 7. (a) The comparison of frequency shift values of UIO-66-SO₃H based QCM sensors to five kinds of vapor (the concentration of all vapor is set as 60 ppb), respectively. (b) Frequency shift data showing the selectivity of UIO-66-SO₃H based QCM sensor when exposed to aniline and interferent BTEX vapors with the concentration of 60 ppb

During the process of adsorptive detection of aniline vapor, it is very important to improve the anti-interference ability of BTEX vapor, including benzene, toluene, ethylbenzene, and xylene vapor. The aniline molecule and the four BTEX molecules have very similar molecular sizes, shapes, and volatility, making it difficult to detect them selectively using an adsorption approach. Consequently, we compared the sensing performance to aniline vapor and BTEX vapor of UIO-66-SO₃H based QCM sensor. The five vapors are all uniformly concentrated at 60 ppb. As shown in Figure 7a, the frequency shift of UIO-66-SO₃H based QCM sensor to aniline vapor, benzene vapor, toluene vapor, ethylbenzene vapor, and xylene vapor are -7.6 Hz, 1.6 Hz, 1.8 Hz, 1.9 Hz and 2.0 Hz, respectively. It is obvious that there is significant difference between these five frequency shifts, which reflects the selective detection ability of UIO-66-SO₃H based QCM sensor to aniline vapor against BTEX vapor. The UIO-66-SO₃H based QCM sensor's superiority in selective aniline detection over BTEX vapor should be credited to its acid -SO₃H group, which can introduce acid-base interaction with the -NH₂ group in aniline structure.

To further evaluate the practical selectivity, the UIO-66-SO₃H based QCM sensor was subjected to an aniline vapor including four interfering BTEX vapors, including benzene vapor, toluene vapor, ethylbenzene vapor, and xylene. All five vapors have a uniform concentration of 60 ppb. The corresponding frequency shift data are listed in Figure 7b. The frequency shift of UIO-66-SO₃H based QCM sensor to aniline vapor is 7.9 Hz. It should be noted that after we introduced other vapor into aniline vapor, although the response increased, the increase was not significant, demonstrating remarkable selectivity against other interfering BTEX compounds. Furthermore, compared to aniline vapor (7.9 Hz), the frequency shift to a mixture of four interfering BTEX vapors (2.5 Hz) is quite low. The above research results show that the UIO-66-SO₃H based QCM aniline sensor has a clear advantage in terms of resistance to BTEX vapor.

CONCLUSIONS

In conclusion, UIO-66-SO₃H is synthesized and first developed as a mass-sensitive material for ppb level aniline detection. The prepared UIO-66-SO₃H loaded Quartz Crystal Microbalance (QCM) sensor possesses obvious frequency shift to ppb level aniline vapor. There is a Langmuir relationship between the frequency shift and aniline concentration in the 20-120 ppb aniline concentration range. Based on experimental results, the UIO-66-SO₃H loaded sensor shows excellent selectivity to ten kinds of common interfering gases, as well as BTEX vapor, and its ability to detect aniline is stable under different humidity. The repeatability and stability of the sensor are

also favorable. This research supports the potential for MOF materials in high-performance gas sensing.

SUPPLEMENTARY MATERIAL

In supplementary material, available on <http://quimicanova.s bq.org.br> as a PDF file, with free access, are presented the fabrication and test method of QCM sensor and schematic of the sensing testing system (Figure 1S).

ACKNOWLEDGEMENTS

This research was supported by National Natural Science Foundation of China under Grant No. 62001420, Zhejiang Provincial Natural Science Foundation of China (No. LQ21F010017), and Science Foundation of Zhejiang Gongshang University Hangzhou College of Commerce, Zhejiang Gongshang University, China (ZJHZCC) under Grant No. 2222111.

REFERENCES

- Jagadeesh, R. V.; Surkus, A. E.; Junge, H.; Pohl, M. M.; Radnik, J.; Rabeah, J.; Huan, H.; Schuenemann, V.; Brueckner, A.; Beller, M.; *Science* **2013**, *342*, 1073. [Crossref]
- Alghamdi, Y. G.; Rub, M. A.; Azum, N.; Asiri, A. M.; *J. Phys. Org. Chem.* **2021**, *34*, e4120. [Crossref]
- Maliyappa, M. R.; Keshavayya, J.; Mallikarjuna, N. M.; Pushpavathi, I.; *J. Mol. Struct.* **2020**, *1205*, 127576. [Crossref]
- Kovacic, P.; Somanathan, R.; *MedChemComm* **2011**, *2*, 106. [Crossref]
- Deng, L.; Yuan, J.; Huang, H.; Xie, S.; Xu, J.; Yue, R.; *Food Chem.* **2022**, *372*, 131212. [Crossref]
- Chang, J.; Meng, H.; Li, C.; Gao, J.; Chen, S.; Hu, Q.; Li, H.; Feng, L.; *Adv. Mater. Technol.* **2020**, *5*, 1901087. [Crossref]
- Wang, B.; He, R.; Xie, L. H.; Lin, Z. J.; Zhang, X.; Wang, J.; Huang, H.; Zhang, Z.; Schanze, K. S.; Zhang, J.; Xiang, S.; Chen, B.; *J. Am. Chem. Soc.* **2020**, *142*, 12478. [Crossref]
- Lu, B.; Li, P.; Li, P.; Zhang, Y.; Muellen, K.; Yin, M.; *J. Mater. Chem. C* **2020**, *8*, 1421. [Crossref]
- Chen, M.; Zhu, G.; Wang, S.; Jiang, K.; Xu, J.; Liu, J.; Jiang, J.; *J. Sep. Sci.* **2018**, *41*, 440. [Crossref]
- Bakier, Y. M.; Ghali, M.; Elkun, A.; Beltagi, A. M.; Zahra, W. K.; *Mater. Res. Bull.* **2021**, *134*, 111119. [Crossref]
- Lee, C. H.; Hsu, L. Y.; Lien, C. Y.; Huang, P. Y.; Yang, J. S.; *J. Chin. Chem. Soc.* **2020**, *67*, 1957. [Crossref]
- Wang, D.; Zhang, D.; Guo, J.; Hu, Y.; Yang, Y.; Sun, T.; Zhang, H.; Liu, X.; *Nano Energy* **2021**, *89*, 106410. [Crossref]

13. Li, P.; Yu, J.; Cao, C.; Song, W.; *Chem. Res. Chin. Univ.* **2021**, *37*, 1317. [Crossref]
14. Wang, R.; Yu, X.; Li, Z.; Chen, J.; Jiang, T.; *Chem. Res. Chin. Univ.* **2021**, *37*, 584. [Crossref]
15. Zhang, Y. H.; Wang, C. N.; Gong, F. L.; Wang, P.; Guharoy, U.; Yang, C.; Zhang, H. L.; Fang, S. M.; Liu, J.; *J. Hazard. Mater.* **2020**, *388*, 122069. [Crossref]
16. Zhang, Y. H.; Peng, M. X.; Yue, L. J.; Chen, J. L.; Gong, F. L.; Xie, K. F.; Fang, S. M.; *J. Alloys Compd.* **2021**, *885*, 160988. [Crossref]
17. Gong, F.; Wang, Y.; Gong, L.; Sun, Y.; Wang, P.; Zhang, Y.; Li, F.; *Mater. Lett.* **2021**, *304*, 130636. [Crossref]
18. Lv, Y.; Yu, H.; Xu, P.; Xu, J.; Li, X.; *Sens. Actuators, B* **2018**, *256*, 639. [Crossref]
19. Ma, Y.; Chen, X.; Bai, J.; Yuan, G.; Ren, L.; *Inorg. Chem. Commun.* **2019**, *100*, 64. [Crossref]
20. Babaei, H.; Eslami, M. R.; *Int. J. Mech. Mater. Des.* **2021**, *17*, 381. [Crossref]
21. Sheng, N.; Ji, P.; Zhang, M.; Wu, Z.; Liang, Q.; Chen, S.; Wang, H.; *Adv. Electron. Mater.* **2021**, *7*, 2001235. [Crossref]
22. Yu, Y.; Zheng, G.; Dai, K.; Zhai, W.; Zhou, K.; Jia, Y.; Zheng, G.; Zhang, Z.; Liu, C.; Shen, C.; *Mater. Horiz.* **2021**, *8*, 1037. [Crossref]
23. Cai, G.; Yan, P.; Zhang, L.; Zhou, H. C.; Jiang, H. L.; *Chem. Rev.* **2021**, *121*, 12278. [Crossref]
24. Ren, J.; Chang, M.; Zeng, W.; Xia, Y.; Liu, D.; Maurin, G.; Yang, Q.; *Chem. Mater.* **2021**, *33*, 5108. [Crossref]
25. Lai, C.; Wang, Z.; Qin, L.; Fu, Y.; Li, B.; Zhang, M.; Liu, S.; Li, L.; Yi, H.; Liu, X.; Zhou, X.; An, N.; An, Z.; Shi, X.; Feng, C.; *Coord. Chem. Rev.* **2021**, *427*, 213565. [Crossref]
26. Xu, H.; Zhong, F.; Chen, F.; Luan, T. X.; Li, P.; Xu, S.; Gao, J.; *J. Mater. Chem. C* **2022**, *10*, 7469. [Crossref]
27. Gao, J.; Cai, Y.; Qian, X.; Liu, P.; Wu, H.; Zhou, W.; Liu, D. X.; Li, L.; Lin, R. B.; Chen, B.; *Angew. Chem., Int. Ed.* **2021**, *60*, 20400. [Crossref]
28. Martinez-Ahumada, E.; Diaz-Ramirez, M. L.; Velasquez-Hernandez, M. d. J.; Jancik, V.; Ibarra, I. A.; *Chem. Sci.* **2021**, *12*, 6772. [Crossref]
29. Zhao, Y.; Liu, J.; Han, M. L.; Yang, G. P.; Ma, L. F.; Wang, Y. Y.; *Rare Met.* **2021**, *40*, 499. [Crossref]
30. Zhao, X.; Zheng, M.; Gao, X.; Zhang, J.; Wang, E.; Gao, Z.; *Coord. Chem. Rev.* **2021**, *440*, 213970. [Crossref]
31. Campbell, M. G.; Sheberla, D.; Liu, S. F.; Swager, T. M.; Dinca, M.; *Angew. Chem., Int. Ed.* **2015**, *54*, 4349. [Crossref]
32. Alev, O.; Sarica, N.; Ozdemir, O.; Arslan, L. C.; Buyukkose, S.; Ozturk, Z. Z.; *J. Alloys Compd.* **2020**, *826*, 154177. [Crossref]
33. Nyang'au, W. O.; Kahmann, T.; Viereck, T.; Peiner, E.; *Chemosensors* **2021**, *9*, 207. [Crossref]
34. Buecken, G.; Koerner, J.; *J. Microelectromech. Syst.* **2020**, *29*, 1032. [Crossref]
35. Kadirsoy, S.; Atar, N.; Yola, M. L.; *New J. Chem.* **2020**, *44*, 6524. [Crossref]
36. Fang, H.; Lin, J.; Hu, Z.; Liu, H.; Tang, Z.; Shi, T.; Liao, G.; *Sens. Actuators, B* **2020**, *304*, 127313. [Crossref]
37. Chen, Q.; Huang, X. H.; Yao, Y.; Luo, K. B.; Pan, H. Z.; Wang, Q.; *IEEE Sens. J.* **2021**, *21*, 22450. [Crossref]
38. Cai, S.; Li, W.; Xu, P.; Xia, X.; Yu, H.; Zhang, S.; Li, X.; *Analyst* **2019**, *144*, 3729. [Crossref]
39. Haghighi, E.; Zeinali, S.; *Microporous Mesoporous Mater.* **2020**, *300*, 110065. [Crossref]
40. Yang, X. L.; Zang, R. B.; Shao, R.; Guan, R. F.; Xie, M. H.; *J. Hazard. Mater.* **2021**, *413*, 125467. [Crossref]
41. Haghighi, E.; Zeinali, S.; *RSC Adv.* **2019**, *9*, 24460. [Crossref]
42. Lv, Y.; Xu, P.; Yu, H.; Xu, J.; Li, X.; *Sens. Actuators, B* **2018**, *262*, 562. [Crossref]
43. Aghakhani, A.; Mohamadi, F.; Ghadimi, J.; *Int. J. Environ. Anal. Chem.* **2021**, *101*, 1803. [Crossref]
44. Jasuja, H.; Peterson, G. W.; Decoste, J. B.; Browe, M. A.; Walton, K. S.; *Chem. Eng. Sci.* **2015**, *124*, 118. [Crossref]
45. Xu, T.; Shehzad, M. A.; Wang, X.; Wu, B.; Ge, L.; Xu, T.; *Nano-Micro Lett.* **2020**, *12*, 1. [Crossref]
46. Gul, S.; Latafat, K. R.; Asma, M.; Ahmad, M.; Kilic, Z.; Zafar, M.; Ding, Y.; Malik, A.; *Microsc. Res. Tech.* **2022**, *85*, 1289. [Crossref]
47. Wang, L.; Wang, Z.; Xiang, Q.; Chen, Y.; Duan, Z.; Xu, J.; *Sens. Actuators, B* **2017**, *248*, 820. [Crossref]
48. Ahmadijokani, F.; Mohammadkhani, R.; Ahmadi-pouya, S.; Shokrgozar, A.; Rezakazemi, M.; Molavi, H.; Aminabhavi, T. M.; Arjmand, M.; *Chem. Eng. J.* **2020**, *399*, 125346. [Crossref]
49. Lv, S. W.; Liu, J. M.; Li, C. Y.; Ma, H.; Wang, Z. H.; Zhao, N.; Wang, S.; *New J. Chem.* **2019**, *43*, 7770. [Crossref]
50. Li, K.; Lin, S.; Li, Y.; Zhuang, Q.; Gu, J.; *Angew. Chem., Int. Ed.* **2018**, *57*, 3439. [Crossref]
51. Wang, L.; Xu, J.; Wang, X.; Cheng, Z.; Xu, J.; *Sens. Actuators, B* **2019**, *288*, 289. [Crossref]